Nano World Journal

https://doi.org/10.17756/nwj.2023-s5-012

Research Article

Open Access

Charge-plasma Persuaded Underlapping Dielectric Modulated Bio-tunnel FET Realizing Repulsive Steric Effect

Amit Bhattacharyya[1], Ayush Sarkar[2], Swapnendu Sarkar[2], Shristi Das[2], Soumyadeep Ghosh[2], Papiya Debnath[3], Debashis De[4] and Manash Chanda[2*]

[1]Department of Electronics and Communication Engineering, Haldia Institute of Technology, Haldia, West Bengal, India
[2]Department of Electronics and Communication Engineering, Meghnad Saha Institute of Technology, Kolkata, West Bengal, India
[3]Department of Basic Science and Humanities, Techno International New Town, Kolkata, West Bengal, India
[4]Department of Computer Science and Engineering, Maulana Abul Kalam Azad University of Technology, Kolkata, West Bengal, India

***Correspondence to:**
Manash Chanda
Department of Electronics and Communication Engineering,
Meghnad Saha Institute of Technology,
Kolkata, West Bengal, India.
E-mail: manash.chanda.1983@ieee.org

Received: October 11, 2023
Accepted: December 18, 2023
Published: December 21, 2023

Citation: Bhattacharyya A, Sarkar A, Sarkar S, Das S, Ghosh S, et al. 2023. Charge-plasma Persuaded Underlapping Dielectric Modulated Bio-tunnel FET Realizing Repulsive Steric Effect. *NanoWorld J* 9(S5): S62-S66.

Copyright: © 2023 Bhattacharyya et al. This is an Open Access article distributed under the terms of the Creative Commons Attribution 4.0 International License (CCBY) (http://creativecommons.org/licenses/by/4.0/) which permits commercial use, including reproduction, adaptation, and distribution of the article provided the original author and source are credited.

Published by United Scientific Group

Abstract

Here, charge-plasma (CP) underlapping dielectric modulated tunnel FET supported biosensor (U-CP-DM-Bio-TFET) is offered. The variations of biomolecular permittivity (k) and charge density (N_f), nanogap dimensions (L_{cavity}, T_{cavity}) at different drain/source potential (V_{ds}) influence ON-state current (I_{ON}), as well as sensitivity. Moreover, repulsive steric effects (RSE) inside nanogap sections can diminish the gap among theoretical and practical surroundings. ATLAS device simulator is employed to authenticate the working capacity of the suggested model. It has been examined that the suggested model might be a probable contestant supporting label-free biosensor realizing RSE matter. Recommended model presents almost 69% imprecision in I_{ON} as allowing for RSE perspective.

Keywords

Doping-less, Dopant fluctuation, Repulsive steric effect, Sensitivity, Tunneling

Introduction

To overcome the drawbacks of bulk MOSFET based biosensor [1, 2] due to incessant down scaling, Bio-tunnel FET (TFET) [2, 3] has been employed like an appropriate contender which recommend improved sensitivity, little reliance of fill-factor, with speedy response time due to band-to-band tunneling incident (BTBT) [3]. Conversely, along with most recent issued literature reviews, TFET bears harsh difficulties akin to low I_{ON} as silicon reliance's exponentially upon the band gap and effectual mass, effect of ambipolarity and random-dopant-fluctuations (RDFs) [4, 5]. Alongside, it is hard in TEFT structures for doping of source/drain and abrupt intersections [6] by complex thermal budgeting formats [7].

RDF [8, 9] generates changes in the threshold voltage (V_{TH}), turn-on potential as well as subthreshold swing (SS) [9-11] in TFET. Hence, RDF influences the sensitivity factors (ΔV_{TH}, ΔI_{ON}) of the Bio-TFET mainly. To reduce the influences of RDF, CP-TFET [12, 13] is initiated presently. Here, first U-CP-TFET architecture is incorporated to illustrate the efficiency of the structure in relation to presented literature. Next, U-CP-DM-Bio-TFET has been suggested to enhance ΔV_{TH}, ΔI_{ON} of the label-free biosensing design.

The recommended U-CP-TFET configuration and the consequent calibrated I_D-V_G characteristics [14] are depicted in figure 1a and 1b. Here, roughly <

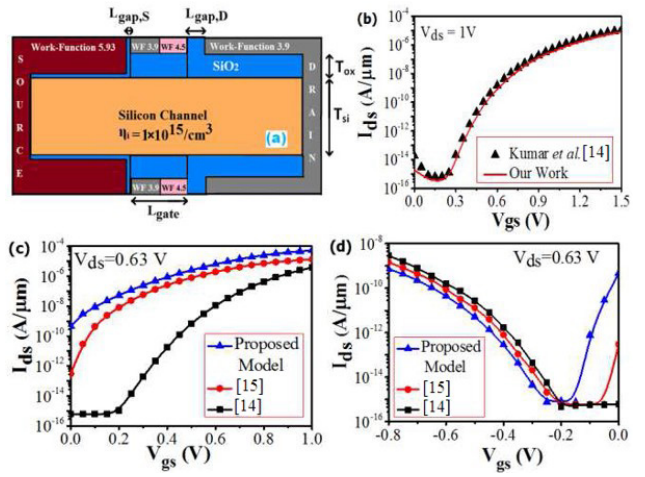

Figure 1: (a) Schematic of cavity free U-CP-TFET and **(b)** Proposed model regulated (I_{ds}-V_{gs} features) along with the simulated verifications in [14]. Estimation of I_{ds}-V_{gs} features of U-CP-TFET respecting other TFET structures with **(c)** positive and **(d)** negative V_{gs}.

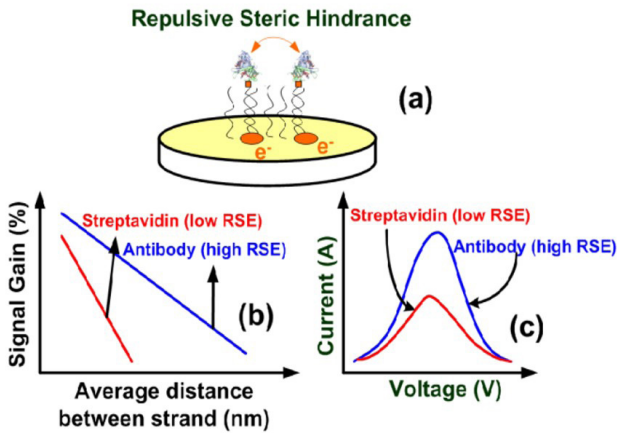

Figure 2: (a) Diagram of RSE on bio-analytes. Impact of RSE on **(b)** signal gaining and **(c)** initiated current for streptavidin with antibody.

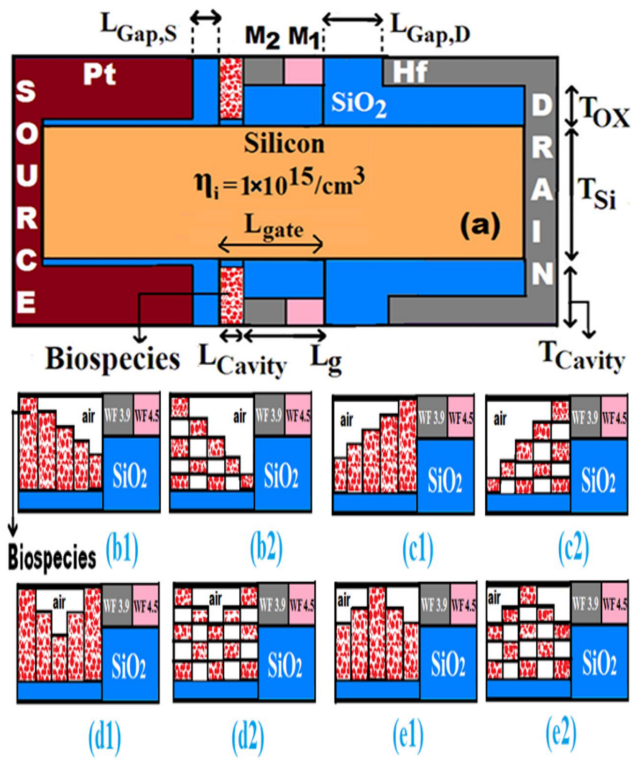

Figure 3: (a) Schematic of U-CP-DM-Bio-TFET. Representation of **(b1, b2)** decreasing, **(c1, c2)** increasing, **(d1, d2)** concave, **(e1, e2)** convex step orientations of bio-analytes in cavity following SE with RSE.

10% inaccuracy has been viewed in I_{ON}. Figure 1c explains the advance in I_D-V_G aspects of the proposed model respecting published works [14, 15] at V_{ds} = 0.63 V and reaches utmost I_{ON} (≈ 53.8 μA/μm). Figure 1d specifies the sub-V_{TH} performance of U-CP-TFET. U-CP-TFET behaves as a possible contender for energy proficient purpose due to less DIBL, low SS, and superior I_{ON}. Since the dual-metal-gate advances transfer of mobile carrier, transconductance, and output impedence for drain extensively, hence, analog presentation of U-CP-TFET is better with dual-metal-gate [15] rather than utilizing a single-metal-gate [14].

Immobilization and hybridization of biomolecules via receptors or else probes hamper the further entrance of bioanalytes inside the cavity owing to RSE [16] mainly. The graphical illustration of RSE is depicted in figure 2a. This too explains the biomolecules binding possibility via the efficient peripheral. The signal gain too reduces [16] for poor binding. RSE consequence on signal spreading out with initiated current is exposed in figure 2b and 2c.

U-CP-TFET has been reorganized via removing particular section of dielectric layer, to accomplish U-CP-DM-Bio-TFET as label free bio-sensor. Schematic of U-CP-DM-Bio-TFET is exposed in figure 3a. While the common researchers have scrutinized totally filled nanogap [15], we stress upon the asymmetrical conformity of bioanalytes in the nanogap, accomplishing poor binding prospects, exterior functionality [3], etc.

In realism, the RSE does not consent two alike charged biomolecules put in closeness inside the nanogap. Thus, considerations of diverse irregular step profiles throughout simulation are supposed in the nanogap as exhibited in figure 3b to 3e.

Experimentation

Structural explanations and process of simulation

International Technology Roadmap for Semiconductors [17] recommends the architectural design of proposed model with dual-gate agreement to merely achieve the device-phase simulation framework [18]. Various device design factors are depicted in table 1. For DL structure, p^+ (n^+)-regions are formed by introducing platinum (Hafnium) metal plate having ϕ_m = 5.92 (3.91) eV close to the S/D [13]. For silicon body thickness (T_{Si}) < 0.010 μm, quantum mechanical effect (QME) suits critical. Owing to QME, V_{TH} as well as surface potential alters [15]. Moreover, QME affects SS and tunneling rate. Hence, to evade QME, T_{Si} = 10 nm [14, 15, 19] is assumed all through during simulations. Here, SiO_2 film evades leakage for G/Ch and provides glue layer for bio-analytes hybridization also [3].

Table 1: Design factors.

Parameters	Values
Silicon film thickness (T_{Si})	0.010 μm
Length of nanogap (L_{cavity})	0.075 μm
Extent of overlap segment for gate (L_g)	0.043 μm
Channel (Ch) doping concentration (η_i)	10^{15}/cm^3
Cavity thickness (T_{cavity})	0.015 μm
SiO_2 layer width near gate (T_{ox})	0.012 μm
spacing thickness of gate (G)/source (S) ($L_{gap,S}$) and gate (G)/drain (D) ($L_{gap,D}$)	0.003 μm, 0.015 μm
Work function of dual metal	3.9 eV, 4.5 eV
Oxide thickness near source (drain) part	0.0005 μm, 0.012 μm

Silvaco ATLAS two-dimensional mathematical device simulator [20], V5.19.20 has been utilized to carry out the simulation of the recommended model. Here, various models akin to nonlocal type of BTBT, Shockley-Read-Hall, CVT-Lombardi, field-dependence mobility (FLD-MOB), and FD statistics are considered. Here, Biotins (k ≈2.63) and APTES (k ≈3.57) are utilized likely linking through bioreceptor to confine Streptavidin (k ≈2.1 likely biotarget [21].

The complete process of biosensing is reviewed in [22]. Charged bioanayte has both k and charge (N_f), likely non-hybridized SS-DNA [23]. Here, $N_f \approx 0/cm^2$, $\pm 5 \times 10^{11}/cm^2$, $\pm 1 \times 10^{12}/cm^2$ are considered as the charges for oxide during simulation. Here, k = 1 signifies the empty cavity and the charged bioanalytes existence inside the nanogap outcomes flat-band voltage (qN_f/C) improvement [16]. Figure 4 reveals feasible manufacturing scheme about U-CP-DM-Bio-TFET.

Capacitance modeling carried SE and RSE

SE (steric effect) as well as RSE influenced capacitive modeling within the cavity is explained in figure 5a and 5b accomplishing the decreased step-profile. Here, bifurcation of cavity keen on 5-by-5 order matrix has been chosen with an area of (A x 1/5) and thickness of (d x 1/5) unit of every tiniest segment respectively. The resultant capacitance for every stripe is set as, $(C_s)^{-1} = (m_s/C_{Bio}) + (n_s/C_V)$, where $m_s(n_s)$ indicates quantity of fully (vacant) status in every stripe and $C_V(C_{Bio})$ denotes capacitance for vacuum (fill-up) area. Here, $C_V = \varepsilon_v(A \times 1/5)/(d \times 1/5)$ and $C_{Bio} = k\varepsilon_v (A \times 1/5)/(d \times 1/5)$, while ε_v indicates permittivity of vacuum. Hence, $C_s = kC_V/(m_s + kn_s) = C_V Z_s$, while $Z_s = k/(m_s + kn_s)$. Now, the resultant capacitance owing to SE inside the gap is as:

$$C_{res,SE} = \sum_{s=1}^{5} C_V Z_s = C_V \left[\frac{k}{5} + \frac{k}{1(k+4)} + \frac{k}{2(k+3/2)} + \frac{k}{3(k+2/3)} + \frac{k}{4(k+1/k)} \right] \quad (1)$$

In concern through RSE in the gap, the resultant capacitance is stated as:

$$C_{res,RSE} = \sum_{s=1}^{5} C_V Z_s = C_V \left[\frac{k}{2k+3} + \frac{2k}{3(k+2/3)} + \frac{k}{4(k+1/4)} \right] \quad (2)$$

- Formation of SiO_2/Si stack1 and stack2 using Atomic Layer Deposition (ALD) by depositing SiO_2 on Si wafer
- Chemical etching of bottom Si layer by iterative thermal oxidation and wet chemical etching process by buffered oxide etchant (BOI), four times, to get SiO_2/Si structure1 and structure2
- Fusion wafer bonding to obtain SiO_2/Si/SiO_2 configuration by inverting SiO_2/Si structure1 on SiO_2/Si structure2
- Post bonding annealing at lower temperature
- Source electrode recognition through creating window by selective etching of SiO_2 from source side utilizing Buffered HF solution
- Pt sputtering through creating window to induce hole plasma in undoped silicon
- Creating window after selective etching of SiO_2 from drain side using HF solution
- Hf sputtering through creating window to induce electron plasma in undoped silicon
- Both top and bottom side Metal1 (M_1) deposition by Electron beam evaporation
- Dual side deposition of hard mask (HM), defining M_1 region via lithography and selectively etching out the HM/ M_1 from unwanted area (i.e., other side)
- M_1- M_2 dual metal gate configuration by depositing Metal2 (M_2) on both sides
- Cavity formation on both sides by vertical etching of selected portion of SiO_2

Figure 4: Feasible manufacturing scheme about U-CP-DM-Bio-TFET.

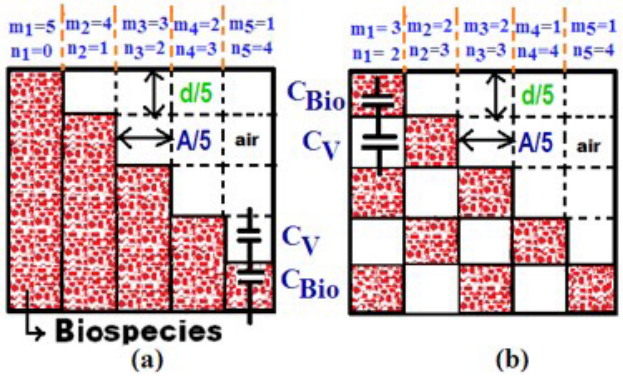

Figure 5: Representation of the compacted capacitive modeling about **(a)** SE and **(b)** RSE inside the nanogap.

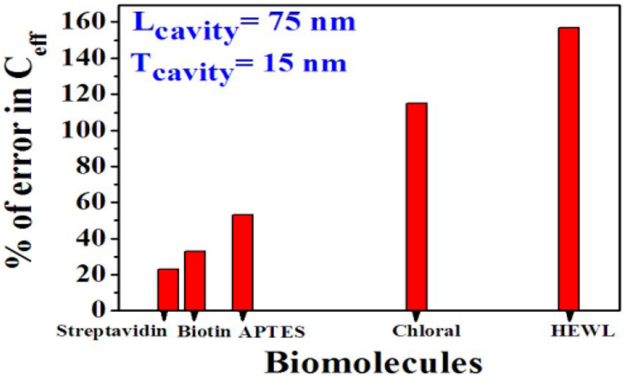

Figure 6: Percentage of inaccuracy in self-assuming SE.

Figure 6 shows the evaluation of percentage of inaccuracy in resultant capacitance (C_{res}) estimation for diverse bioanalytes devoid of RSE in the usual model. Moreover, superior *k* can initiate further inaccuracies in result. Besides, owing to

this incorrect C_{res}, minimum detected charge, $Q_{bio,min.}$ (= C_{res} x $\Delta\phi_{min.}$) needs manipulation, whereas $\Delta\phi$ indicates an alter in surface potential (ψ). Thus, to estimate exact sensitivity factors, RSE requires to be comprised in biosensing purposes.

Results and Discussion

Performance Analysis Through RSE

Performance study of suggested biosensor is emphasized here. A decreased step-profile through an RSE approach has been employed all through the simulation. Hence, neutral biomolecules (k ≈ 2.1, 2.63, 3.57) and N_f = ±1 x 10^{16}/m^2, ± 5 x 10^{15}/m^2 [16] are presumed as charge-based biomolecules exist in the gap.

Influence of neutral/charged biomolecules on Ids

Influence of neutral biomolecules

Assessment of I_{ds} with RSE approach of bio-molecules within the nano-gap having L_{cavity} of 75 nm at V_{ds} = 0.63 V is shown in figure 7a. Suggested model achieves utmost I_{ON} above [15]. I_{ON} increases as k of neutral bioanalytes rises inside the nanogap since a further band-bending next to S/Ch intersection is viewed [16]. Besides, 72% (105%) enhancement concerning [15] is obtained while Streptavidin (APTES) exists assuming RSE approach as evidenced in figure 7a.

Influence of charged biomolecules

The outcome on S/Ch barrier thickness reduction is viewed from figure 7b. Moreover, respecting neutral biomolecule (k = 2.1), negatively and positively charged biomolecule diminishes and enhances I_{ON} as exposed here. Furthermore, for the existence of charged biomolecules with N_f = +1 x 10^{16}/m^2, 0/m^2, and -1 x 10^{16}/m^2 assuming RSE approach, nearly 40%, 29%, and 58% enhancement respecting [15] has been achieved as shown in figure 7b. This is owing to lessening (improvement) to S/Ch barrier thickness while biomolecules with +ve (-ve) charged immobilize in the nanogap.

Impact upon I_{ON} and S_{ION}

Effect upon I_{ON}

The reliance of channel section upon gate segment raises and therefore I_{ON} increases [4-6, 14] after the accumulation of bioanalytes (k >1) within the nanogap. Figure 8a shows while L_{cavity} enhances, the C_{res} diminishes and I_{ON} begins to lessen [4-6]. Here, U-CP-DM-Bio-TFET achieves utmost I_{ON} of ~ 6.1 µA/µm while k = 3.57 with L_{cavity} = 75 nm through SE and gives 69% inaccuracy for allowing RSE scheme. Figure 8b exposes that I_{ON} reduces (enhances) for –ve (+ve) charged biomolecules with N_f = ±1 x 10^{16}/m^2, ±5 x 10^{15}/m^2. In incidence of ±N_f change in qN_f/C_{res} drives ψ to vary. Hence, I_{ON} alters too. Here, I_{ON} reaches an utmost of 6.5 µA/µm while N_f = +1 x 10^{16}/m^2 having SE scheme inside the gap for L_{cavity} = 75 nm and gives 103% inaccuracy when considering the offered RSE scheme.

Effect upon S_{ION}

Now, S_{ION} = (I_{ON}^{bio} - I_{ON}^{air})/ I_{ON}^{air}, [1] while I_{ON}^{bio}, I_{ON}^{air} represents current under ON-condition in aid of full and unfilled gap. Figure 8c illustrates that S_{ION} improves for rising of k of neutral biomolecules in the nanogap [14] and shows an utmost inaccuracy of ~ 53%, 67% amongst SE and RSE schemes with L_{cavity} = 0.075 µm, 0.090 µm correspondingly. This is owing to the decrease of S/Ch barrier thickness and thus S_{ION} rises. Moreover, a maximum enrichment of S_{ION} of ≈ 50% has been attained with k = 3.57 having SE over vacuum for L_{cavity} of 75 nm. Furthermore, S_{ION} attains an utmost enrichment of ~ 66.5% with N_f = +1 x 10^{16}/m^2 concerning k = 1 as shown in figure 8d. This is because of lessening (enrichment) of S/Ch barrier thickness for bioanalytes of +ve (-ve) charged in the cavity. Finally, Figure 8a to 8d ensures that the charge-persuaded Bio-TFET is more efficient than neutral-based contender. Moreover, +vely charged bioanalytes offer superior sensitivity over its -ve counterpart.

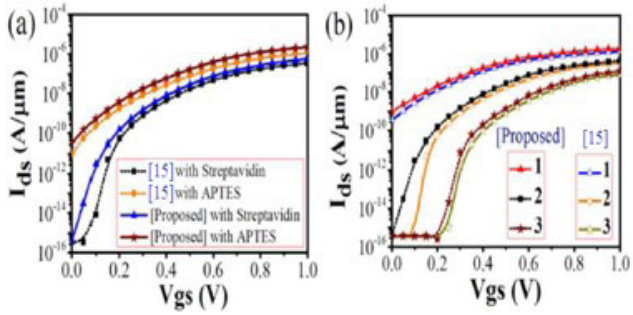

Figure 7: Comparison of I_{ds}-V_{gs} features of upside [15] and up-down section [offered] of S/D segment for **(a)** neutral biomolecules and **(b)** charged bio-analytes (bio-target) by RSE approach at V_{ds} of 0.63V, L_{cavity} of 0.075 µm. Now, 1: N_f of +1 x 10^{16}/m^2, 2: N_f of 0, 3: N_f of -1 x 10^{16}/m^2.

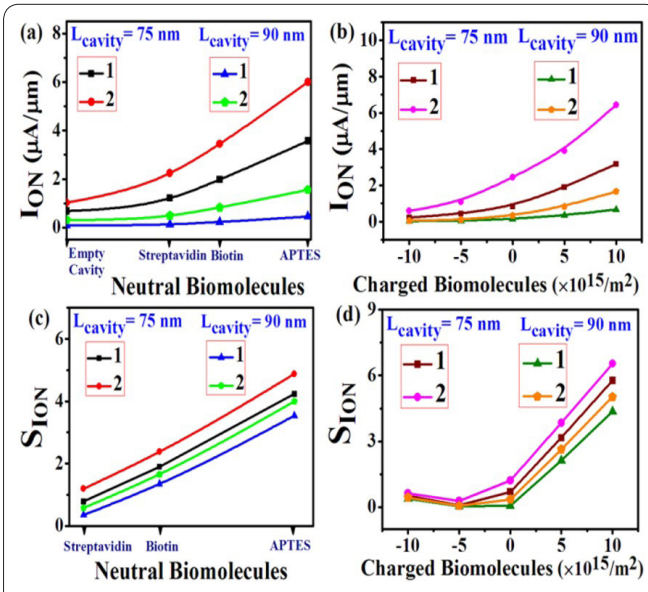

Figure 8: Assessment of **(a)** I_{ON}: neutral, **(b)** I_{ON}: charged, **(c)** S_{ION}: neutral, and **(d)** S_{ION}: charged bio-analytes for L_{cavity} = 0.075 µm, 0.090 µm of offered model. Now, 1: RSE, 2: SE.

Conclusion

An inclusive analysis of U-CP-DM-Bio-TFET is highlighted here. The variations of k and N_f, L_{cavity}, T_{cavity} at differ-

ent V_{ds} influence I_{ON}, as well as sensitivity. Furthermore, RSE inside the cavity is initiated to scrutinize partly hybridization scheme. Lastly, the analysis ensures that the charge-based Bio-TFET is more efficient than neutral-based contender and obviously +vely charged bioanalytes offer superior sensitivity over its -ve counterpart. Consequently, the suggested model offers enhanced aspects as biosensor.

Acknowledgments

None.

Conflict of Interest

None.

References

1. Bhattacharyya A, Chanda M, De D. 2019. Performance assessment of new dual-pocket vertical heterostructure tunnel FET-based biosensor considering steric hindrance issue. *IEEE Trans Electron Dev* 66(9): 3988-3993. https://doi.org/10.1109/TED.2019.2928850
2. Bhattacharyya A, Banerjee M, Debnath P, De D, Chanda M. 2022. RF/analog performance analysis of electrostatically doped dual pocket vertical tunnel field effect transistor. In IEEE VLSI Device Circuit and System, Kolkata, West Bengal, India.
3. Bhattacharyya A, Chanda M, De D. 2020. Analysis of noise-immune dopingless heterojunction bio-TFET considering partial hybridization issue. *IEEE Trans Nanotech* 19: 769-777. https://doi.org/10.1109/TNANO.2020.3033966
4. Nigam K, Pandey S, Kondekar PN, Sharma D, Parte PK. 2017. A barrier controlled charge plasma-based TFET with gate engineering for ambipolar suppression and RF/linearity performance improvement. *IEEE Trans Electron Dev* 64(6): 2751-2757. https://doi.org/10.1109/TED.2017.2693679
5. Narang R, Saxena M, Gupta M. 2015. Comparative analysis of dielectric-modulated FET and TFET-based biosensor. *IEEE Trans Nanotech* 14(3): 427-435. https://doi.org/10.1109/TNANO.2015.2396899
6. Jhaveri R, Nagavarapu V, Woo JC. 2010. Effect of pocket doping and annealing schemes on the source-pocket tunnel field-effect transistor. *IEEE Trans Electron Dev* 58(1): 80-86. https://doi.org/10.1109/TED.2010.2089525
7. Ionescu AM, Riel H. 2011. Tunnel field-effect transistors as energy-efficient electronic switches. *Nature* 479: 329-337. https://doi.org/10.1038/nature10679
8. Bhattacharyya A, Pachal P, Pradhan A, Chanda M, De D. 2019. Performance analysis of underlap double gate oxide stacked junctionless MOSFET for analog and RF applications. In International Conference on Microwave Integrated Circuits, Photonics and Wireless Networks, Tiruchirappalli, Tamil Nadu, India.
9. Bhattacharyya A, De D, Chanda M. 2023. Ovarian-cancer biomarker (HE4) recognition in serum using hetero TFET biosensor. *IEEE Trans Nanotech* 22: 238-244. https://doi.org/10.1109/TNANO.2023.3272926
10. Roy S, Jana G, Chanda M. 2022. Analysis of sub-threshold adiabatic logic model using junctionless MOSFET for low power application. *Silicon* 14(3): 903-911. https://doi.org/10.1007/s12633-020-00870-y
11. Sarkar A, De S, Chanda M, Sarkar CK. 2016. Low Power VLSI Design: Fundamentals. Walter de Gruyter.
12. Bhattacharyya A, Mukherjee A, Chanda M, De D. 2020. Advantages of charge plasma based double gate junctionless MOSFET over bulk MOSFET for label free biosensing. In IEEE VLSI Device Circuit and System, Kolkata, West Bengal, India.
13. Bhattacharyya A, Chanda M, De D. 2020. $GaAs_{0.5}Sb_{0.5}/In_{0.53}Ga_{0.47}As$ heterojunction dopingless charge plasma-based tunnel FET for analog/digital performance improvement. *Superlattices Microstruct* 142: 106522. https://doi.org/10.1016/j.spmi.2020.106522
14. Kumar MJ, Janardhanan S. 2013. Doping-less tunnel field effect transistor: design and investigation. *IEEE Trans Electron Dev* 60(10): 3285-3290. https://doi.org/10.1109/TED.2013.2276888
15. Wadhwa G, Raj B. 2018. Parametric variation analysis of symmetric double gate charge plasma JLTFET for biosensor application. *IEEE Sens J* 18(15): 6070-6077. https://doi.org/10.1109/JSEN.2018.2846409
16. Bhattacharyya A, De D, Chanda M. 2022. Sensitivity measurement for bio-TFET considering repulsive steric effects with better accuracy. *IEEE Trans Nanotech* 21: 100-109. https://doi.org/10.1109/TNANO.2022.3148922
17. Resources. 2013. International Technology Roadmap for Semiconductors (ITRS). [https://www.semiconductors.org/resources/2013-international-technology-roadmap-for-semiconductors-itrs/] [Accessed December 20, 2023]
18. Bhattacharyya A, Chanda M, De D. 2021. Dielectrically Modulated Bio-FET for Label-free Detection of Bio-molecules. In Dutta G, Biswas A, Chakrabarti A (eds) Modern Techniques in Biosensors. Studies in Systems, Decision and Control. Springer, pp 183-198.
19. Bhattacharyya A, De D, Chanda M. 2022. Temperature imposed sensitivity issues of hetero-TFET based pH sensor. *IEEE Trans NanoBiosci* 22(2): 438-446. https://doi.org/10.1109/TNB.2022.3202242
20. ATLAS User's Manual. Device Simulation Software. Silvaco International, Santa Clara, CA.
21. Bhattacharyya A, Chanda M, De D. 2020. Analysis of partial hybridization and probe positioning on sensitivity of a dielectric modulated junctionless label free biosensor. *IEEE Trans Nanotech* 19: 719-727. https://doi.org/10.1109/TNANO.2020.3025544
22. Williams EH, Davydov AV, Motayed A, Sundaresan SG, Bocchini P, et al. 2012. Immobilization of streptavidin on 4H–SiC for biosensor development. *Appl Surf Sci* 258(16): 6056-6063. https://doi.org/10.1016/j.apsusc.2012.02.137
23. Cuervo A, Dans PD, Carrascosa JL, Orozco M, Gomila G, et al. 2014. Direct measurement of the dielectric polarization properties of DNA. *Proc Natl Acad Sci* 111(35): E3624-E3630. https://doi.org/10.1073/pnas.1405702111